3.5 SCCMS Projects

Data Generation for Magnetic Properties at Finite Temperature

Tetsuya FUKUSHIMA
National Institute of Advanced Industrial Science and Technology (AIST)
1-1-1 Umezono, Tsukuba, Ibaraki 305-8568, Japan

The purpose of Data Creation and Utilization-Type Material Research and Development Project (Digital Transformation Initiative Center for Magnetic Materials) is to find new functional magnetic materials by data-driven approaches.

In this year, we developed the the all-electron full-potential Korringa–Kohn–Rostoker (FPKKR) Green's function method which can treat finite temperature effects [1], and systematically investigated how Pr substitution affects the magnetocrystalline anisotropy of $(Nd_{1-x}Pr_x)_2Fe_{14}B$. We present our results on the latter topic in this report. Motivated by experimental observations indicating that local lattice distortions near grain boundaries modify the magnetocrystalline anisotropy, our objective was to clarify the responses of the anisotropy constant K_u and the magnetization J_S to the Pr concentration x and to changes in the lattice constants (the biaxial strain δa and the c-axis strain δc).

For the calculations, we employed the FPKKR method, adopting the local density approximation for the exchange–correlation functional. Spin–orbit coupling was included self-consistently in the total-energy calculations, and the magnetocrystalline anisotropy constant was evaluated from the total-energy difference between the quantization axes along [001] and [100] as

$$K_u = \frac{E_{100} - E_{001}}{V},$$

where V is the unit-cell volume. Substitutional disorder on the rare-earth sublattice was treated within the coherent potential approximation (CPA), and $(Nd_{1-x}Pr_x)_2Fe_{14}B$ was evaluated in steps of $x = 0.1$. The $4f$ orbitals of Nd and Pr were treated as open-core, assuming the trivalent states $Nd^{3+}(4f^3)$ and $Pr^{3+}(4f^2)$. As an initial magnetic configuration, the Fe $3d$ spins and the rare-earth $5d$ spins were set antiparallel, and self-consistent calculations were performed to obtain converged solutions.

Lattice distortions were introduced by varying only the lattice constants a and c while preserving tetragonal symmetry. Assuming tetragonal symmetry, the biaxial strain was defined as

$$\delta a := \delta d_{[110]} = \frac{d_{[110]} - d^{\mathrm{bulk}}_{[110]}}{d^{\mathrm{bulk}}_{[110]}},$$

where $d_{[hkl]}$ denotes the lattice spacing along the $[hkl]$ direction and $d^{\mathrm{bulk}}_{[hkl]}$ is its bulk value. In the Pr-dependence analysis, we mainly compared the x and δa dependences of K_u and J_S under the conditions $\delta c = 0, \pm 3\%$ (Fig. 1).

In the following, we summarize the results obtained as the Pr-substitution effect. First, in the strain-free condition ($\delta c = 0$), the FPKKR calculations estimate $K_u = 6.0$ MJ/m^3 for $Pr_2Fe_{14}B$, which is larger than $K_u = 4.2$ MJ/m^3 for $Nd_2Fe_{14}B$. Moreover, at $\delta c = 0$, K_u increases almost linearly with the Pr concentration x, indicating that Pr addition enhances the anisotropy in the low-temperature regime. In contrast, J_S is slightly smaller on the Pr-rich side, consistent with the smaller

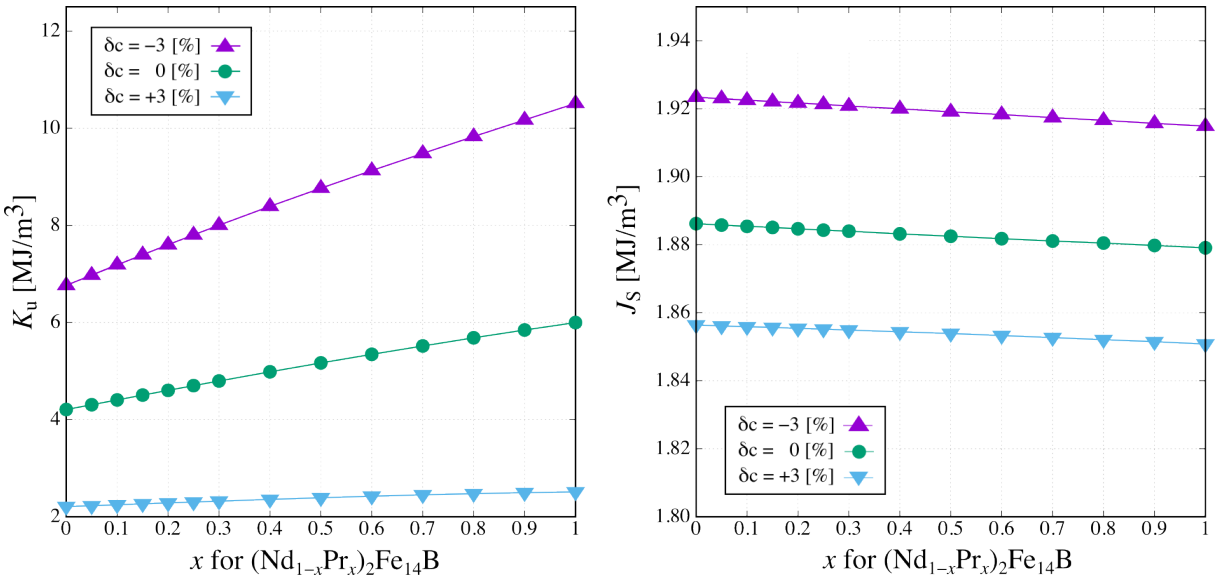

Figure 1: Schematic overview of the Pr-concentration (x) dependence of (a) K_u and (b) J_S in $(Nd_{1-x}Pr_x)_2Fe_{14}B$, and of the changes in K_u and J_S under [110] compression (δa).

effective magnetic moment of Pr^{3+} (3.20 μ_B) compared with Nd^{3+} (3.27 μ_B). Notably, the magnetization (or total magnetic moment) excluding the $4f$ contribution is identical for $Nd_2Fe_{14}B$ and $Pr_2Fe_{14}B$, amounting to 1.57 T (31.9 μ_B/f.u.), confirming that J_S is predominantly governed by Fe.

Next, we compare the response of K_u to uniform biaxial compression ($\delta a < 0$). At $\delta c = 0$, K_u in $Pr_2Fe_{14}B$ decreases with increasing compression, similarly to $Nd_2Fe_{14}B$. The reduction of K_u is more pronounced for Pr-richer compositions: the K_u values of $Pr_2Fe_{14}B$ and $Nd_2Fe_{14}B$ become equal around $\delta a \simeq -4\%$, and under stronger compression the Pr-rich side exhibits smaller K_u. From the viewpoint of crystal-field theory, this difference is attributed to the difference in the Stevens factor α_J (Pr^{3+} : −0.02, Nd^{3+} : −0.006): both have $\alpha_J < 0$ (oblate), but the larger magnitude for Pr^{3+} implies stronger nonsphericity of the $4f$ charge distribution, making K_u more sensitive to lattice distortions. For $\delta c = +3\%$, the decrease in K_u for the Pr-based compound is even stronger: K_u of $Pr_2Fe_{14}B$ becomes negative at approximately $\delta a \simeq -3.5\%$. By contrast, for $\delta c = -3\%$, the reduction of K_u under biaxial compression is partially suppressed, and at least up to $\delta a = -5\%$ the K_u of $Pr_2Fe_{14}B$ remains larger than that of $Nd_2Fe_{14}B$. These results suggest that Pr substitution enhances K_u in strain-free bulk, whereas it can markedly accelerate the reduction of K_u under biaxial compression, especially under conditions with a larger c/a ratio.

Finally, to examine the influence of local site preference, we compared three occupation models in which Pr selectively occupies the $4f$ site, selectively occupies the $4g$ site, or is uniformly distributed over both sites. In all models, K_u increases with increasing Pr concentration, indicating that the trend is robust. For example, at $x = 0.50$, K_u is 5.59, 5.16, and 4.75 MJ/m^3 for the $4f$-selective, uniform, and $4g$-selective models, respectively; although the absolute values differ due to site preference, the qualitative conclusion that Pr substitution enhances K_u in the strain-free case remains unchanged.

References

[1] M. Ogura and H. Akai, *J. Phys. Condens. Matter.* **17**, 5741 (2005).

Finite-Temperature Magnetism of Transition-Metal Alloys Using KKR Green's Function Method

Takashi MIYAKE
Materials DX Research Center, AIST
Umezono, Tsukuba, Ibaraki 305-8568

We have studied finite-temperature magnetism of binary alloys of 3d transition metals using first-principles calculation. This year, we focused on the dependence of the magnetization on the lattice parameters.

The calculation is based on density functional theory. The generalized gradient approximation (GGA) of the Perdew-Burke-Ernzerhof (PBE) type functional is employed for the exchange and correlation energies We assume that the potential of the system is represented as a collection of spherically symmetric mffin-tin potentials. The relativistic effect is considered within the scalar relativistic approximation. We use the AkaiKKR program package. Chemical disorder is treated in the coherent potential approximation (CPA) combined with the Korringa-Kohn-Rostoker (KKR) Green's function method. Finite-temperature effects are included by considering scattering by phonons and magnons in CPA, where lattice displacements and ratio of majority spins to minority spins are adjusted at each temperature. Target material space is selected from the combinations of V, Cr, Mn, Fe, Co, Ni and Cu in the body-centered tetragonal structure with changing c/a and volume. We perform structure optimization for pure Cr, Mn, Fe, Co, Ni, and Cu by using the QUANTUM ESPRESSO package. Then, the lattice parameters of the alloys are determined by the Vegard ' s law.

Figure 1 shows the magnetic moment of binary alloys as a function of the average electron number. At 0 K and $a/a_0 = 1$, the magnetic moment increases with increasing the electron number, then turns to decreases, as is know as the Slater-Pauling curve. The average electron number at which the magnetic moment is maximized decreases (increases) as a/a_0 increases (decreases). Similar trend is observed at finite temperatures. With increasing temperature, the magnetic moment decreases and the peak position is shifted to larger electron number.

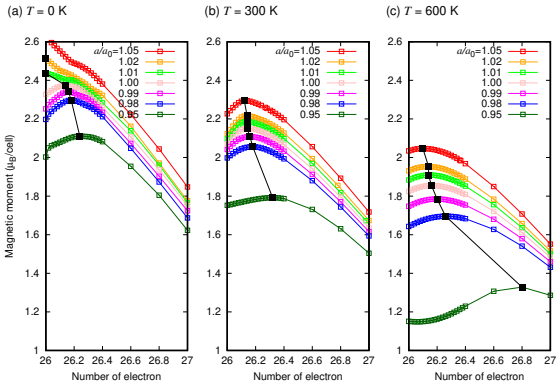

Figure 1: Calculated Slater-Pauling curve at 0 K, 300 K, 600 K. The lattice constant is varied to see volume dependence of the Slater-Pauling curve.

References

[1] Reo Kita, Taro Fukazawa, Takashi Miyake, and Tetsuya Fukushima: Materials Research Meeting 2025.

Chiral Effects on Aqueous Solubility of Polypeptides Explored by Molecular Simulations

Kazuo Yamada and Nobuyuki Matubayasi

Division of Chemical Engineering Science, Graduate School of Engineering Science, The University of Osaka, Toyonaka, Osaka 560-8531, Japan

Background

Partial substitution of L-amino-acid residues by their mirror-image D counterparts is a promising strategy for improving the proteolytic stability of peptide drugs. In contrast, the effect of such stereochemical modification on water solubility remains poorly understood. In particular, it is still unclear whether the solubility change is governed simply by the number of D residues or by the detailed L/D substitution pattern along the chain. Here we address this issue for Ala homopolypeptides by combining all-atom molecular dynamics (MD) simulations of the aqueous and peptide-solid phases with free-energy calculations. The present report focuses on the results for the tetrapeptides, while calculations for 8- and 12-residue systems are in progress.

Methods

Ala homotetrapeptides with several L/D substitution patterns were constructed by molecular modeling. For each pattern, all-atom MD simulations were carried out in liquid water and in the peptide solid phase. GROMACS (ver. 2022.4) was used for MD sampling, and ERmod (ver. 1.0.4) was used for free-energy analysis. As a thermodynamic proxy for water solubility, we evaluated the transfer free energy $\Delta G^{\mathrm{tr}} = \mu_{\mathrm{liq}}^{\mathrm{solv}} - \mu_{\mathrm{solid}}^{\mathrm{solv}}$; a more negative value indicates higher water solubility. To identify the physical origin of the pattern dependence, the solvation free energy was decomposed within the ERmod framework as

$$\mu^{\mathrm{solv}} = \langle v \rangle + \mu^{\mathrm{excl}} + \mu^{\mathrm{re-org}},$$

where $\langle v \rangle$ is the direct solute-solvent interaction term, μ^{excl} is the excluded-volume term, and $\mu^{\mathrm{re-org}}$ is the solvent-reorganization term in the low-energy region.

Results and Discussion

Figure 1 shows the L/D-pattern dependence of the calculated solubility proxy for Ala homotetrapeptides. The LLLL, DLLL, and DLLD patterns exhibit similar values of ΔG^{tr}, indicating only a slight change in water solubility. In contrast, the alternating LDLD pattern gives a distinctly more negative ΔG^{tr} and therefore a marked enhancement of water solubility. These results show that the stereochemical arrangement along the chain, rather than the mere presence of D residues, is the decisive factor. We also performed the ERmod free-energy decomposition. The dominant contribution to the LDLD enhancement is the reduction in the solvent-reorganization term $\mu^{\mathrm{re-org}}$ between the liquid and solid phases. By contrast, the difference in μ^{excl} is small, showing that the improvement does not originate from a substantial change in molecular size. The direct interaction term $\langle v \rangle$ also contributes, but less significantly than $\mu^{\mathrm{re-org}}$.

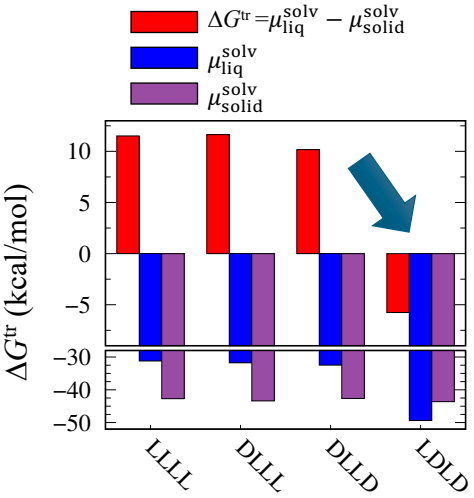

Figure 1: Pattern dependence of $\mu_{\mathrm{liq}}^{\mathrm{solv}}$, $\mu_{\mathrm{solid}}^{\mathrm{solv}}$, and ΔG^{tr} for Ala homotetrapeptides.

These results suggest that the LDLD pattern induces a solution structure that lowers the solvent-reorganization penalty without greatly changing the effective peptide size. For Ala homotetrapeptides, the alternating L/D pattern is therefore a favorable motif for water solubility. Ongoing calculations for longer Ala homopolypeptides will test how general this mechanism is.

Passivation in Sn-Based Perovskites and Interpretable Machine Learning Approaches

Tomomi Shimazaki

Graduate School of Nanobioscience,

Yokohama City University, 22-2 Seto, Kanazawa, Yokohama 236-0027

In this study, we investigated the passivation of surface tin-vacancy defects in Sn-based mixed-halide perovskites, focusing on materials with different bromine concentrations.[1-2] These wide-bandgap perovskites are promising for tandem solar cell applications. We found that Lewis base molecules effectively suppress deep p-type defect states on perovskite surfaces. These defects were attributed to halide dimer structures, indicating that strong interactions between passivating molecules and surface halide dimers are required for effective passivation. The results are consistent with previous studies on related Sn-based perovskite systems. Overall, this work provides guidance for molecular surface passivation strategies and supports the rational design of perovskite materials for photovoltaic applications, although further microscopic studies on bromine-containing films are needed.

In addition, we developed a modified convex clustering (regression) method in which representative points are selected directly from the training dataset.[3] By varying the number of representative points, the method enables control over both data representation and model complexity. Applying this approach to acrylate (ACR) and methyl acrylate (MA) radical reaction datasets, we constructed machine learning models for predicting reaction energy barriers and observed improved prediction accuracy with more representative points. Because these points are real data samples used directly in the prediction process, the models are highly interpretable. This framework offers a promising approach for analyzing chemical reaction data and other complex scientific datasets.

References

[1] E. Kino, M. Takagi, M. Tachikawa, K. Yamashita, and T. Shimazaki, *J. Chem. Phys.,* 163, 104703 (2025).

[2] E. Kino, M. Takagi, M. Tachikawa, K. Yamashita, and T. Shimazaki, *Phys. Chem. Chem. Phys*., 27, 7429 (2025).

[3] T. Shimazaki and M. Tachikawa, *Phys. Chem. Chem. Phys.* 28, 2499 (2026).

Numerical Spectroscopy for Cuprate Superconductors

Youhei YAMAJI
Research Center for Materials Nanoarchitectonics (MANA), National Institute for Materials Science (NIMS), Namiki, Tsukuba-shi, Ibaraki 305-0044

To elucidate properties of correlated quantum materials, numerical methods have evolved alongside advances in computing facilities with machine learning [1]. In particular, neural quantum states, such as resonating-valence-bond wavefunctions augmented by neural networks [2], have enabled access to accurate ground state properties of the quantum materials.

Building on this progress, the researchers extend the generator-coordinate method [3, 4, 5] within a flexible variational Monte Carlo framework by incorporating artificial neural networks [2]. This dynamical variational scheme [6, 7] allows unified simulations of a wide range of spectra, including electron energy loss spectroscopy, neutron scattering, (inverse) photoemission, and resonant inelastic neutron scattering.

Applying the method to cuprate superconductors, we show that the characteristic spin-excitation energy extracted from simulated neutron spectra does not correlate with the optimal critical temperature. Figure 1 shows examples of dynamical spin and charge structure factors of $Bi_2Sr_2CuO_6$ (Bi2201) at half filling, which are proportional to the inelastic neutron scattering and electron energy loss spectroscopy spectra, respectively.

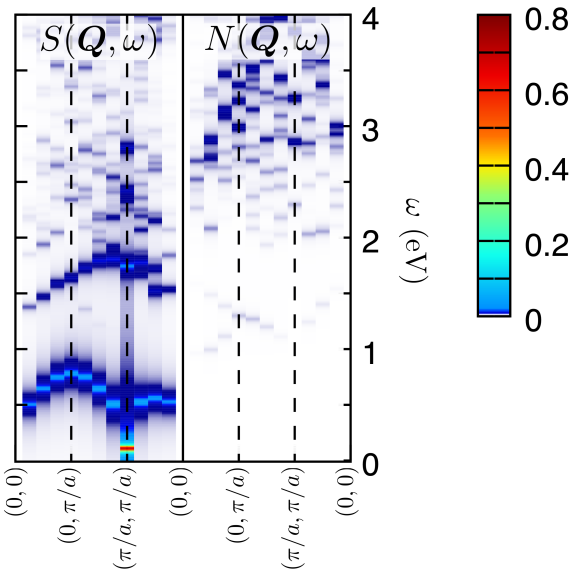

Figure 1: Dynamical spin (charge) structure factors for Bi2201 at half filling shown in the left (right) panel.

References

[1] As a review, H. Lange, *et al.*: Quantum Sci. Technol. **9**, 040501 (2024).

[2] Y. Nomura, *et al.*: Phys. Rev. B **96**, 205152 (2017).

[3] D. L. Hill and J. A. Wheeler: Phys. Rev. **89**, 1102 (1953).

[4] J. J. Griffin and J. A. Wheeler: Phys. Rev. **108**, 311 (1957).

[5] T. Li and F. Yang: Phys. Rev. B **81**, 214509 (2010).

[6] K. Ido, M. Imada, and T. Misawa: Phys. Rev. B **101**, 075124 (2020).

[7] M. Charlebois and M. Imada: Phys. Rev. X **10**, 041023 (2020).